LETTERS

Linear and nonlinear optical spectroscopy of a strongly coupled microdisk–quantum dot system

Kartik Srinivasan[1]† & Oskar Painter[2]

Cavity quantum electrodynamics[1], the study of coherent quantum interactions between the electromagnetic field and matter inside a resonator, has received attention as both a test bed for ideas in quantum mechanics and a building block for applications in the field of quantum information processing[2]. The canonical experimental system studied in the optical domain is a single alkali atom coupled to a high-finesse Fabry–Perot cavity. Progress made in this system[1–5] has recently been complemented by research involving trapped ions[6], chip-based microtoroid cavities[7], integrated microcavity-atom-chips[8], nanocrystalline quantum dots coupled to microsphere cavities[9], and semiconductor quantum dots embedded in micropillars, photonic crystals and microdisks[10–12]. The last system has been of particular interest owing to its relative simplicity and scalability. Here we use a fibre taper waveguide to perform direct optical spectroscopy of a system consisting of a quantum dot embedded in a microdisk. In contrast to earlier work with semiconductor systems, which has focused on photoluminescence measurements[10–14], we excite the system through the photonic (light) channel rather than the excitonic (matter) channel. Strong coupling, the regime of coherent quantum interactions, is demonstrated through observation of vacuum Rabi splitting in the transmitted and reflected signals from the cavity. The fibre coupling method also allows us to examine the system's steady-state nonlinear properties, where we see a saturation of the cavity–quantum dot response for less than one intracavity photon. The excitation of the cavity–quantum dot system through a fibre optic waveguide is central to applications such as high-efficiency single photon sources[15,16], and to more fundamental studies of the quantum character of the system[17].

In the most simplified picture, cavity quantum electrodynamics (cavity QED) consists of a single two-level atom (or equivalent) coupled to an electromagnetic mode of a cavity. A more realistic picture includes dissipative processes, such as cavity loss and atomic decoherence, and excitation of the system, either through the atomic or photonic channel. The observed system response is dependent on both which channel is excited, and what signal is measured. Previous demonstrations of strong coupling between semiconductor microcavities and quantum dots[10–13] used non-resonant optical pumping to excite the quantum dot stochastically and photoluminescence to probe the system behaviour. In this work, we excite the system coherently through the photonic channel, and detect signatures of cavity–quantum dot coupling in the resonant optical response. Such optical spectroscopy is commonplace in atom Fabry–Perot systems[1], but is more problematic in semiconductor microcavities owing to the comparative difficulty in effectively coupling light into and out of submicrometre structures. To effectively interface with the cavity, we use an optical fibre taper waveguide[18]. Fibre tapers are standard glass optical fibres that have been heated and stretched to a diameter that is at or below the wavelength of light, at which point the evanescent field of the guided mode extends into the surrounding air and allows the taper to function as a near-field optic[7,19–21].

The experimental set-up used is shown schematically in Fig. 1a, b. At its core is a customized liquid-helium cryostat[22] in which piezo-actuated stages have been integrated to enable optical fibre taper

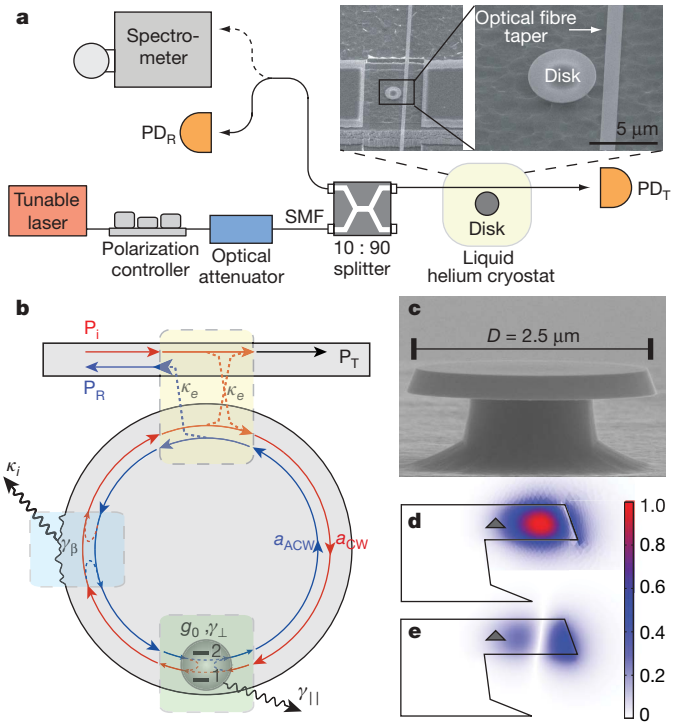

Figure 1 | Experimental apparatus and the cavity–quantum dot system. **a**, Diagram of the experimental set-up, showing a scanning electron microscope (SEM) image of a taper-coupled microdisk. $PD_{R/T}$ are photodetectors for the reflected/transmitted signals and SMF corresponds to single-mode fibre optical links. **b**, Illustration of the coupled microdisk–quantum dot system. Here $a_{CW/ACW}$ are the amplitudes for the clockwise/anticlockwise modes, $P_{i/R/T}$ are the incident/reflected/transmitted signals, and κ_e and κ_i correspond respectively to the fibre-to-cavity coupling and the intrinsic cavity field decay rates. For a standing wave WGM, the loaded cavity field decay rate is $\kappa_T = \kappa_i + 2\kappa_e$. **c**, SEM image of one of the small microdisk cavities under study. **d**, **e**, Finite-element-method simulations of the radial (**d**; E_ρ) and azimuthal (**e**; E_φ) electric field components of the $TE_{p=1,m=13}$ mode in cross-section; p denotes the radial order and m the azimuthal mode number. The fields are normalized to the peak radial electric field strength in the cavity. The shaded triangle indicates the estimated quantum dot position in this work.

[1]Center for the Physics of Information, [2]Thomas J. Watson Sr Laboratory of Applied Physics, California Institute of Technology, Pasadena, California 91125, USA. †Present address: Center for Nanoscale Science and Technology, National Institute of Standards and Technology, Gaithersburg, Maryland 20899, USA.

testing while maintaining a sample temperature as low as 8 K. External cavity tunable lasers optically pump the quantum dot and probe the cavity–quantum dot system near resonance, and fused-fibre couplers direct the cavity's reflected and transmitted signals to photodetectors and a spectrometer. The overall transmission of the fibre taper link is 50% in this work, and in many cases can be >90%, providing a very-low-loss optical channel to probe the system. This allows for the accurate estimation of quantities such as the average intra-cavity photon number through measurement of the resonant transmission of the taper waveguide when coupled to the cavity.

The system under investigation consists of InAs quantum dots embedded in a GaAs microdisk cavity. The InAs quantum dots are grown in a self-assembled manner with a density of $300-500\,\mu m^{-2}$ on top of an InGaAs quantum well (a so-called dot-in-a-well, or DWELL[23]). The DWELL structure resides in the middle of a 256-nm-thick GaAs layer that forms the thin planar layer of the microdisk (Fig. 1c). Previous studies of this material[24] indicate that isolated emission from single quantum dots at cryogenic temperature can be seen in the wavelength range $\lambda = 1{,}290$–$1{,}310$ nm, approximately 50 nm red-shifted from the peak of the quantum dot ensemble emission. Microdisks of diameter $D = 2.5\,\mu m$ are created through electron beam lithography, plasma dry etching, and wet undercut etching[21]. Finite-element-method simulations (Fig. 1d, e) of the microdisks show that the $TE_{1,13}$ whispering gallery mode (WGM) is resonant at $\lambda_0 \approx 1{,}300$ nm. This optical mode has a radiation-limited quality factor of $Q_{rad} > 10^8$ in the absence of material absorption and fabrication-induced roughness in the disk shape, and an effective standing wave mode volume $V_{sw} = 3.2(\lambda_0/n)^3$ for a microdisk refractive index $n \approx 3.4$. The peak coherent coupling rate g_0 between cavity mode and quantum dot for an excitonic state of the type studied here (spontaneous emission lifetime $\tau_{sp} = 1$ ns), with optimal placement and dipole orientation, is $g_0/2\pi = 15$ GHz. Because our quantum dots are not deterministically positioned in the cavity, in contrast to recent studies[25], the actual exhibited coupling rate g may be significantly smaller (see Methods). The magnitude of g relative to the system decay rates, κ_T (cavity field decay) and $\gamma_\perp$ (quantum dot dephasing), determines whether the system lies in the perturbative (weak coupling: $g < (\kappa_T, \gamma_\perp)$) or non-perturbative (strong coupling: $g > (\kappa_T, \gamma_\perp)$) regime of cavity QED[1].

The process by which we identify a suitable device for studying cavity–quantum dot coupling is described in the Methods section. The main panel of Fig. 2a shows the fibre-taper-collected photoluminescence spectrum from one such device that has been cooled down to 15 K. Optical pumping of the quantum dot is provided by exciting (also through the taper) a blue-detuned higher-order WGM of the disk at $\lambda_P = 982.2$ nm. The cavity mode, which is fed by background emission processes[13], is the tall peak at the blue end of the spectrum. The three emission peaks on the red side of the cavity mode are the fine-structure-split[26] neutral single exciton lines, X_a and X_b, and the negatively charged single exciton line, X^-.

Further insight into the coupled cavity–quantum dot system from photoluminescence is masked by the limited resolution of our spectrometer (35 pm). In this case, the interesting behaviour of the cavity–quantum dot coupling can be studied by resonant spectroscopy of the cavity mode using a fibre-coupled, narrowband (linewidth <5 MHz) tunable laser. The inset to Fig. 2a shows the taper's transmission spectrum when it is placed in contact with the side of the microdisk cavity and the cavity modes are detuned from the exciton lines. As has been described in previous work[21], imperfections on the surface of the microdisk couple the initially degenerate travelling-wave WGMs. If the surface-scattering rate γ_β exceeds the total cavity loss rate κ_T, this mode-coupling results in the formation of standing wave modes that are split in frequency. The transmission scan of Fig. 2a inset illustrates this effect in our system, with $TE_{1,\pm13}$ modes appearing as a resonance doublet with splitting $2\Delta\lambda_\beta =$ 31 pm. Each mode has a linewidth of $\delta\lambda = 13$ pm, corresponding to $Q = 10^5$ and $\kappa_T/2\pi = 1.2$ GHz.

To tune the cavity into resonance with the X_a and X_b exciton lines of the quantum dot, we introduce nitrogen (N_2) gas into the cryostat[22,27]. As described in ref. 22 and in Methods, this allows for continuous and repeated tuning of the cavity modes over a 4 nm wavelength range. For the first set of measurements, we operate with an input power of 470 pW so that the system remains in a weak driving regime with the estimated bare-cavity intracavity photon number $n_{cav} = 0.03$. The normalized transmission and reflection spectra over a cavity tuning range of 240 pm are displayed as an intensity image in Fig. 2b, c. Initially, we see a simple shift in the centre wavelength of the cavity doublet mode, but once the cavity mode frequency nears the transition frequency of the higher-energy exciton line (X_a) of the quantum dot, the spectra change dramatically. We see that coupling between the X_a-line and the cavity modes results in a significant spectral splitting (vacuum Rabi splitting) that is evidenced in the characteristic anticrossing within both the transmitted and reflected signals. This anticrossing is indicative of the cavity taking on the character of the quantum dot exciton, and vice versa, when the system becomes strongly coupled. As the cavity is detuned red of the X_a-line, the spectra regain their initial bare-cavity doublet shape. Further tuning brings the cavity modes into resonance with the X_b-line (not shown). Only a small dispersive shift of the cavity modes' frequencies and no anticrossing is observed in this case, indicating that the X_b state is only weakly coupled to the cavity.

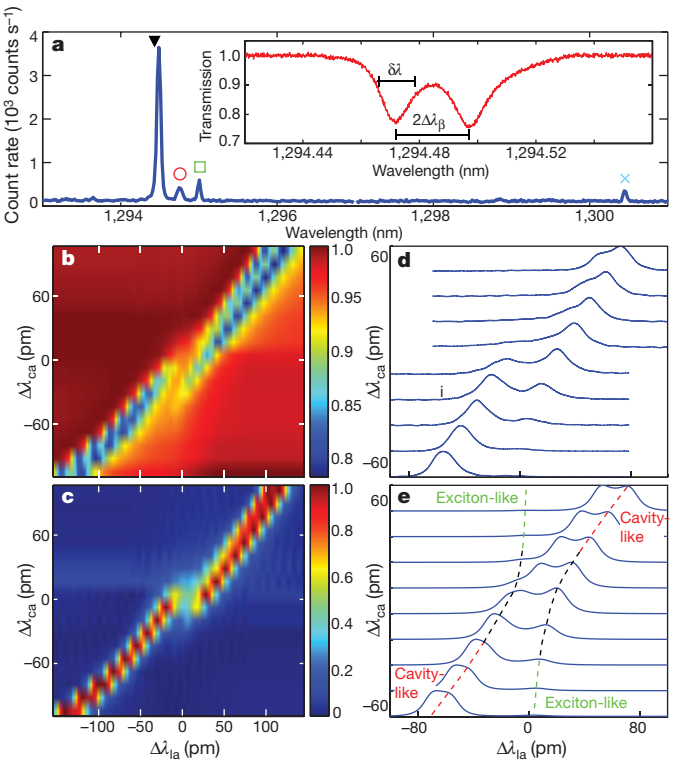

Figure 2 | Reflection and transmission spectra from a strongly coupled microdisk–quantum dot system. **a**, Fibre collected photoluminescence spectrum at a pump power of 30 nW showing the cavity mode (black triangle), X_a (red circle), X_b (green square), and X^- (blue cross) lines. The inset shows a transmission scan of the bare-cavity mode. **b**, **c**, Measured transmission (**b**) and reflection (**c**) spectra as a function of laser–quantum dot detuning ($\Delta\lambda_{la}$) and cavity–quantum dot detuning ($\Delta\lambda_{ca}$), where the cavity wavelength is tuned by the N_2 adsorption. Transmission and reflection spectra are normalized to unity. **d**, **e**, Experimental data (**d**) and model plots (**e**) for a series of reflected spectra in the central 120 pm region of cavity tuning. The dashed lines in **e** are guides to the eye for the exciton-like and cavity-like tuning.

Table 1 | Parameters of quantum master equation model

Parameter	V_{tw}	η	$\kappa_e/2\pi$	$\kappa_i/2\pi$	$\gamma_\beta/2\pi$	ξ	τ_{rad}	$g_{sw1}/2\pi$	$g_{sw2}/2\pi$	$\gamma_\perp/2\pi$	$\gamma_{||}/2\pi$
	$((\lambda_0/n)^3)$		(GHz)	(GHz)	(GHz)	(rad)	(ns)	(GHz)	(GHz)	(GHz)	(GHz)
Value	6.4	0.21	0.171	0.91	1.99	0.25π	1	2.93	1.21	1.17	0.55

Figure 2d shows a series of reflection scans for a zoomed-in region of cavity tuning, near where the X_a-line and the cavity are in resonance. In general, the character of these spectra is complicated by the bimodal nature of WGM cavities. To adequately model the system, we use a quantum master equation[28]. The model is used to solve for the steady-state reflected and transmitted signals from the cavity as a function of parameters such as cavity–exciton coupling and excitonic dephasing (the bare-cavity properties are known from detuned cavity spectra). One other important parameter is the relative phase, ξ, between the surface scattering and exciton mode coupling. The quantum dot–cavity coupling strength with the standing wave modes, $g_{sw1,2}$, is modified relative to that for travelling wave WGMs by a factor of $(1 \pm e^{i\xi})/\sqrt{2}$.

A series of reflected spectra produced by the model is shown in Fig. 2e for a set of parameters, listed in Table 1, which best estimates the measured reflected signal intensity, exciton linewidth, relative coupling to the two standing wave modes, and anticrossed splitting. These parameters place the X_a exciton state and the $TE_{1,13}$ WGM in the good-cavity limit ($g > \gamma_\perp > \kappa_T$) of the strong coupling regime. We note that the achieved g_{sw1} is about five times smaller than the maximum possible value based on the cavity mode volume, and is probably due to the quantum dot position being suboptimal. We estimate that the quantum dot is located 300–400 nm inwards from the position of peak field strength of the $TE_{1,13}$ mode (Fig. 1d), with the dipole moment of the X_a-line oriented radially and that of the X_b-line oriented azimuthally. This picture is consistent with the orthogonal X_a–X_b polarizations[26] and their relative measured coupling strengths.

The rate at which a single exciton can scatter incoming cavity photons is limited, resulting in a saturation in the strongly coupled quantum dot–cavity response for large enough input power. Two parameters used to characterize nonlinear processes in cavity QED are the critical atom number N_0 and the saturation photon number m_0, which respectively gauge the number of atoms needed to alter the cavity response and the number of photons needed to saturate the atomic transition[1]. These parameters are given by $N_0 = 2\kappa_T\gamma_\perp/g^2$ and $m_0 = \gamma_{||}\gamma_\perp/4g^2$, where $\gamma_{||}$ and $\gamma_\perp$ are the exciton energy decay rate and total dipole dephasing rate, respectively. In our system, $N_0 = 0.44$ and $m_0 = 0.02$ for the standing wave mode (sw1) that couples most strongly to the quantum dot. This indicates that a single quantum dot strongly affects the cavity response (which Fig. 2 clearly indicates), while even an average intracavity photon number that is less than one can saturate the quantum dot response.

The measured power dependence of the quantum dot–cavity system is shown in Fig. 3, where the cavity is tuned into resonance with the X_a-line near the centre of the anticrossing region (scan marked 'i' in Fig. 2d), at which point the resonance peaks are nearly equal mixtures of exciton and cavity mode. Figure 3a shows a plot of the measured reflected signal normalized to input power (ΔR) along with the modelled steady-state response of the cavity under weak driving conditions ($n_{cav} = 0.03$). As the input power to the cavity increases, Fig. 3b shows that the spectral splitting due to cavity–quantum dot interaction ($2\Delta\lambda_g$) begins to diminish as the exciton saturates, and finally reaches a regime where the splitting is nearly half as large and due to surface scattering ($2\Delta\lambda_\beta$). Figure 3c plots the resulting mode splitting ($2\Delta\lambda_{g/\beta}$) and peak ΔR as a function of the optical drive power. Both the measured splitting and reflected signal begin to saturate towards their bare-cavity values for $n_{cav} \gtrsim 0.1$. The model based on the quantum master equation (dotted lines) predicts very similar behaviour, with a smooth, extended region of saturation, as expected for a single dipole with quantum fluctuations[3,29].

Use of an optical-fibre-based waveguide to efficiently probe the microcavity–quantum dot system opens up many interesting possibilities for future devices and studies. In particular, excitation and collection through the optical channel allows for high resolution spectral and temporal studies of individual quantum dot dynamics and a direct probe of the intra-cavity field. Studies of the quantum fluctuations of the strongly coupled system[17], through field and intensity correlations of the optical signal, are also now possible. An immediate application is the creation of an efficient fibre-coupled single-photon source, whereas from a long-term perspective, the fibre interface could perhaps serve as a means to transfer quantum information to and from the quantum dot. In comparison, atomic systems have the considerable advantages of homogeneity, much lower dephasing, and an energy level structure compatible with more complex manipulations of the quantum system. Nitrogen-vacancy centres in diamond[9,30] have been viewed as a system that can provide

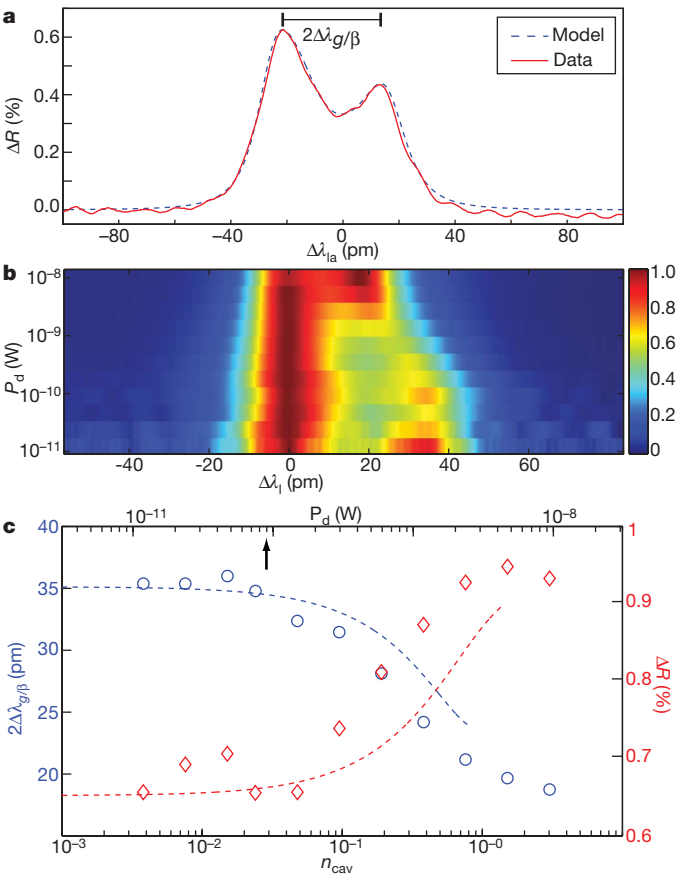

Figure 3 | Power dependence of the quantum dot–microcavity system. **a**, Reflection spectrum from the quantum dot–microdisk system near resonance (position 'i' in Fig. 2) under weak driving. The solid red line is the measured reflected power normalized to input power; the dashed blue line is a quantum master equation model of the system. **b**, Normalized (to unity) reflected signal of **a** as a function of drive strength (dropped power in the bare cavity, P_d) and detuning from the short-wavelength resonance peak ($\Delta\lambda_l$). **c**, Measured and modelled saturation of the mode splitting and peak reflected signal level versus drive strength (n_{cav} (bottom axis); P_d (top axis)). The model is only plotted up to a drive power of $n_{cav} = 1$ owing to size limitations on the cavity mode Fock space that can be simulated. Bold arrow indicates the drive strength used for **a** and Fig. 2b–e.

some of the beneficial aspects of cold atoms. The measurement apparatus described here is equally applicable to this and other systems, and we are hopeful that it can be built on to further progress the development of solid-state cavity QED nodes with microchip scalability.

METHODS SUMMARY

Device identification consists of the following procedure. An array of 50 microdisks is fabricated per sample, with disk diameter nominally equal to $D = 2.5\,\mu m$. Nanometre-scale fluctuations in disk diameter cause the $TE_{1,13}$ mode wavelength to vary over a 1,290–1,310 nm range from device to device in the array. Each microdisk is optically pumped through the fibre taper and on resonance with one of its WGMs in the 980 nm wavelength band[24]. This selectively excites quantum dots that lie in the disk periphery and overlap with the $TE_{1,13}$ mode. For those devices in which isolated quantum dot emission is observed, we examine the spectral position of the $TE_{1,13}$ mode relative to the quantum dot states through photoluminescence and cavity transmission. A digital wet etching process[25] provides a cavity mode blue shift of 0.8 nm per cycle. This wet etch is repeated until the cavity mode, of a chosen device on the sample, lies blue (and within 1 nm) of the desired quantum dot exciton lines. N_2 adsorption is then used to red-shift the mode into resonance with a given exciton line.

The numerically calculated travelling wave mode volume of the $TE_{1,13}$ WGM is $V_{tw} = 6.4(\lambda_0/n)^3$ for the $D = 2.5\,\mu m$ microdisks studied in this work. The coherent coupling rate of the exciton to the travelling wave mode is given by $g_{tw} = \eta(3c\lambda_0^2/8\pi n^3\tau_{sp}V_{tw})^{1/2}$, where η accounts for the position and orientation of the exciton dipole ($\eta = 1$ for an exciton dipole oriented parallel with, and positioned at, the peak of the cavity mode electric field).

Full Methods and any associated references are available in the online version of the paper at www.nature.com/nature.

Received 23 July; accepted 11 September 2007.

1. Kimble, H. J. Strong interactions of single atoms and photons in cavity QED. *Phys. Scripta T* **76,** 127–137 (1998).
2. Mabuchi, H. & Doherty, A. C. Cavity quantum electrodynamics: coherence in context. *Science* **298,** 1372–1377 (2002).
3. Hood, C. J., Chapman, M. S., Lynn, T. W. & Kimble, H. J. Real-time cavity QED with single atoms. *Phys. Rev. Lett.* **80,** 4157–4160 (1998).
4. Hennrich, M., Legero, T., Kuhn, A. & Rempe, G. Vacuum-stimulated Raman scattering based on adiabatic passage in a high-finesse optical cavity. *Phys. Rev. Lett.* **85,** 4872–4875 (2000).
5. Boca, A. *et al.* Observation of the vacuum Rabi spectrum for one trapped atom. *Phys. Rev. Lett.* **93,** 233603 (2004).
6. Keller, M., Lange, B., Hayaska, K., Lange, W. & Walther, H. Continuous generation of single photons with controlled waveform in an ion-trap cavity system. *Nature* **431,** 1075–1078 (2004).
7. Aoki, T. *et al.* Observation of strong coupling between one atom and a monolithic microresonator. *Nature* **443,** 671–674 (2006).
8. Colombe, Y. *et al.* Strong atom-field coupling for Bose-Einstein condensates in an optical cavity on a chip. Preprint at ⟨http://arxiv.org/abs/0706.1390⟩ (2007).
9. Park, Y.-S., Cook, A. K. & Wang, H. Cavity QED with diamond nanocrystals and silica microspheres. *Nano Lett.* **6,** 2075–2079 (2006).
10. Reithmaier, J. P. *et al.* Strong coupling in a single quantum dot-semiconductor microcavity system. *Nature* **432,** 197–200 (2004).
11. Yoshie, T. *et al.* Vacuum Rabi splitting with a single quantum dot in a photonic crystal nanocavity. *Nature* **432,** 200–203 (2004).
12. Peter, E. *et al.* Exciton photon strong-coupling regime for a single quantum dot embedded in a microcavity. *Phys. Rev. Lett.* **95,** 067401 (2005).
13. Hennessy, K. *et al.* Quantum nature of a strongly coupled single quantum dot-cavity system. *Nature* **445,** 896–899 (2007).
14. Khitrova, G., Gibbs, H. M., Kira, M., Koch, S. W. & Scherer, A. Vacuum Rabi splitting in semiconductors. *Nature Phys.* **2,** 81–90 (2006).
15. Michler, P. *et al.* A quantum dot single-photon turnstile device. *Science* **290,** 2282–2285 (2000).
16. Santori, C., Fattal, D., Vuckovic, J., Solomon, G. & Yamamoto, Y. Indistinguishable photons from a single-photon device. *Nature* **419,** 594–597 (2002).
17. Birnbaum, K. M. *et al.* Photon blockade in an optical cavity with one trapped atom. *Nature* **436,** 87–90 (2005).
18. Knight, J. C., Cheung, G., Jacques, F. & Birks, T. A. Phase-matched excitation of whispering-gallery-mode resonances by a fiber taper. *Opt. Lett.* **22,** 1129–1131 (1997).
19. Spillane, S. M., Kippenberg, T. J., Painter, O. J. & Vahala, K. J. Ideality in a fiber-taper-coupled microresonator system for application to cavity quantum electrodynamics. *Phys. Rev. Lett.* **91,** 043902 (2003).
20. Srinivasan, K., Barclay, P. E., Borselli, M. & Painter, O. Optical-fiber-based measurement of an ultrasmall volume, high-*Q* photonic crystal microcavity. *Phys. Rev. B* **70,** 081306R (2004).
21. Srinivasan, K. *et al.* Optical loss and lasing characteristics of high-quality-factor AlGaAs microdisk resonators with embedded quantum dots. *Appl. Phys. Lett.* **86,** 151106 (2005).
22. Srinivasan, K. & Painter, O. Optical fiber taper coupling and high-resolution wavelength tuning of microdisk resonators at cryogenic temperatures. *Appl. Phys. Lett.* **90,** 031114 (2007).
23. Liu, G. T. *et al.* The influence of quantum-well composition on the performance of quantum dot lasers using InAs/InGaAs dots-in-a-well (DWELL) structures. *IEEE J. Quant. Electron.* **36,** 1272–1279 (2000).
24. Srinivasan, K., Painter, O., Stintz, A. & Krishna, S. Single quantum dot spectroscopy using a fiber taper waveguide near-field optic. *Appl. Phys. Lett.* **91,** 091102 (2007).
25. Badolato, A. *et al.* Deterministic coupling of single quantum dots to single nanocavity modes. *Science* **308,** 1158–1161 (2005).
26. Kulakovski, V. D. *et al.* Fine structure of biexciton emission in symmetric and asymmetric CdSe/ZnSe single quantum dots. *Phys. Rev. Lett.* **82,** 1780–1783 (1999).
27. Mosor, S. *et al.* Scanning a photonic crystal slab nanocavity by condensation of xenon. *Appl. Phys. Lett.* **87,** 141105 (2005).
28. Srinivasan, K. & Painter, O. Mode coupling and cavity-quantum-dot interactions in a fiber-coupled microdisk cavity. *Phys. Rev. A* **75,** 023814 (2007).
29. Savage, C. M. & Carmichael, H. J. Single-atom optical bistability. *IEEE J. Quant. Electron.* **24,** 1495–1498 (1988).
30. Santori, C. *et al.* Coherent population trapping of single spins in diamond under optical excitation. *Phys. Rev. Lett.* **97,** 247401 (2006).

Acknowledgements We thank S. Krishna and A. Stintz for providing quantum dot material growth. This work was supported by the Charles L. Powell Foundation and the Center for the Physics of Information at Caltech.

Author Contributions Both K.S. and O.P. contributed to all aspects of this work.

Author Information Reprints and permissions information is available at www.nature.com/reprints. Correspondence and requests for materials should be addressed to O.P. (opainter@caltech.edu).

METHODS

Cavity tuning. Nitrogen is released into the chamber in discrete 5 s increments, with the flow rate adjusted so that a tuning level of ~10 pm per step is achieved. At temperatures above 28 K, the N_2 can be removed from the disk surface and the cavity mode reset back to its original wavelength, allowing for repeated tuning cycles.

Transmission/reflection measurements. A narrowband single-mode laser (linewidth < 5 MHz) with continuous wavelength tuning in the $\lambda = 1{,}300$ nm band is used to probe the cavity–quantum dot system. The transmitted and reflected laser signals are detected by thermal-electric-cooled (1 kHz bandwidth) and liquid-nitrogen-cooled (150 Hz bandwidth) InGaAs photodetectors, respectively. The photodetected signals are low-pass filtered (30 Hz cut-off) and the wavelength scans are averaged 10–20 times to produce the spectra of Fig. 2. Photoluminescence is dispersed through a 550 mm Czerny–Turner spectrometer and detected on a 512 element liquid-nitrogen-cooled InGaAs array (25 μm × 500 μm pixel size yields a resolution of 35 pm).

Quantum master equation simulations. Reference 28 presents an appropriate model for our system. We numerically solve the steady-state quantum master equation for the system's density matrix, from which the transmitted and reflected spectra from the cavity are generated. A Fock space dimension of 6 for each cavity mode was used in modelling the drive power dependence of the system shown in Fig. 3. The expectation of the commutation between creation and annihilation operators for each mode was calculated to ensure accuracy of the simulation.